

FIBER REINFORCED WET-MIX SHOTCRETE UNDER IMPACT

By P. Gupta,¹ N. Banthia,² and C. Yan³

ABSTRACT: As a result of excavation blasting, traffic, sudden ground movements, rock bursts, and seismic activity, shotcrete is often subjected to impact and other dynamic loads. Limited data exist, however, with regard to the resistance of shotcrete to such dynamic loads. Impact resistance of wet-mix shotcrete reinforced with 10 different types of fibers was investigated using instrumented drop weight impact tests. A direct comparison was made with the quasi-static response. Both beam and plate specimens were tested and the data were correlated. Fiber reinforcement was found to be highly effective in improving the fracture energy absorption and toughness under impact loading, but the improvements under impact loading were found to be substantially different than those seen in quasi-static tests, and were also highly dependent on the type of fiber used. When beams and plates were compared, the relative improvements between fiber types were found not necessarily in agreement.

INTRODUCTION

Shotcrete linings in rock stabilization and underground support construction in mines and tunnels are highly susceptible to impact loads caused by blasting or rock bursts (Kirsten 1997). An improved energy absorption capability or toughness under both static and impact load applications is the most important contribution of fiber reinforcement (Banthia et al. 1989, 1996), and in the case of shotcrete, the enhanced toughness and deformability are of particular benefit given the severe deformations imposed on shotcrete linings in service.

Most of the impact studies to date have dealt with cast concrete (Banthia et al. 1989, 1996), and only limited understanding exists of the resistance of shotcrete with or without fiber reinforcement to impact and other dynamic loads. Due to its unique compaction dynamics, fiber and aggregate rebounds, and the preferential in situ orientation of fibers, shotcrete is different from cast concrete (Banthia et al. 1994) and a verbatim application of our understanding of cast concrete to shotcrete is not fully justified.

In most applications, shotcrete is applied as a surface coating or lining that typically remains in a state-of-plane stress, under the action of biaxial, in-plane bending moments and out-of-plane torsional moments. Clearly, the standardized tests that utilize a simple beam specimen loaded under a quasi-static load may not capture the true performance of shotcrete in service. The beam test, however, is a popular test given that it is simple and inexpensive. The type of specimen that should be used for characterizing toughness of fiber reinforced shotcrete, therefore, remains a subject of active debate, and both beam ("Standard" 1994) and plate specimens (European 1996; Bernard 1997) continue to be recommended.

The purpose of the present study was to examine the behavior of fiber reinforced shotcrete beams and plates under impact loading using instrumented drop-weight impact machines and compare it with their static response. The ultimate goal is to develop tough and durable shotcrete materials and support systems for mines and tunnels, especially where rock-bursts are a common occurrence.

SPECIMEN PREPARATION

In all, ten different commercially available shotcrete fibers (Fig. 1) were investigated in wet-mix shotcrete. Note in Fig. 1 that fibers F4 and F5 are identical and different notations are used only to indicate different fiber volume fractions. The ten fibers included: four deformed steel fibers (F1, F2, F3, and F11), two straight polypropylene fibers (F4 and F6), one crimped polypropylene fiber (F7), two straight carbon microfibers (F8 and F9), and one deformed polyvinyl alcohol, PVA, fiber (F10). These fibers were included in wet-mix shotcrete at manufacturers' recommended dosage rates. Two mix proportions were used in this study: one for shotcrete with carbon microfiber without the large aggregates, and the other a routine shotcrete mix for the other fibers including the control (Table 1). Fiber volume fraction in the design mix and in the in-place shotcrete are also reported in Table 1. The difference between these two quantities expresses the fiber rebound for the various fibers.

Shotcrete was produced using a wet-mix rotary equipment (model ALIVA-262) with a 10 L, 12-pocket rotor. Mixes were shot onto prepared wooden forms (600 × 500 × 100 mm) with tapered sides inside a closed shooting chamber using a 350 cu ft/min air flow (100 cu ft/min = 0.05 m³/s). A 5 m long, 50 mm internal diameter hose, and a rotor speed of 4.7 m³/h were used throughout. Rebound on the floor of the chamber was collected and analyzed.

Seven panels were shot for each mix. After 24 h, panels were demoulded and cured in water for an additional 27 days at about 23°C. For each mix, two panels were sawn to obtain eight 100 × 100 × 350 mm beam specimens, the third panel was cored to obtain four cylinders (85 mm ϕ × 100 mm) for compression testing. The remaining four panels were sawn to obtain four plates of 350 × 350 × 100 mm size. Of the eight beams, four were tested under static loading, and the other four were tested under impact loading. Of the four plates, two were tested statically, and the other two were tested under impact loading.

TEST PROCEDURE

Static Tests

The 100 × 100 × 350 mm beam specimens were tested in four-point flexure on a span of 300 mm in accordance with ASTM C 1018-96 ("Standard" 1996) using a 150 kN floor-mounted Instron testing machine. Net deflections of the beam were recorded by installing a yoke around the specimen ("Method" 1984; Banthia and Trottier 1995). In a test, the load was applied at a stress-rate of ≈ 0.012 MPa/s, which corresponds to an applied strain rate of $\approx 2.9 \times 10^{-7}$ /s.








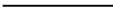

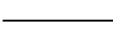
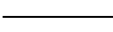
The static tests on plates were performed using a 400,000 lb (1,784 kN) large universal testing machine. The plates were

¹Grad. Res. Asst., Dept. of Civ. Engrg., Univ. of British Columbia, Vancouver, BC, Canada, V6T 1Z4.

²Prof., Dept. of Civ. Engrg., Univ. of British Columbia, Vancouver, BC, Canada, V6T 1Z4.

³Res. Assoc., Dept. of Civ. Engrg., Univ. of British Columbia, Vancouver, BC, Canada, V6T 1Z4.

Note. Associate Editor: David A. Lange. Discussion open until July 1, 2000. To extend the closing date one month, a written request must be filed with the ASCE Manager of Journals. The manuscript for this paper was submitted for review and possible publication on August 19, 1998. This paper is part of the *Journal of Materials in Civil Engineering*, Vol. 12, No. 1, February, 2000. ©ASCE, ISSN 0899-1561/00/0001-0081-0090/\$8.00 + \$.50 per page. Paper No. 19066.

Fiber Shape	Fiber Code	Geometry	Material	Cross Section	Length (mm)	Diameter (mm)	Tensile Strength (MPa)	Fiber Weight (mg)	Elastic Modulus (GPa)
	F1	Hooked-End	Steel	Circular	30	0.5	1115	44.74	210
	F2	Hooked-End	Steel	Circular	35	0.55	1115	63.16	210
	F3	Flat-End	Steel	Circular	30	0.73	1110	95.54	210
	F4*	Straight	Polypropylene	Circular	25	0.38	375	2.75	2.6
	F5*	Straight	Polypropylene	Circular	25	0.38	375	2.75	2.6
	F6	Straight	Polypropylene	Circular	38	0.63	375	10.66	2.6
	F7	Crimped	Polypropylene	Circular	30	0.76	450	21.48	3.5
	F8	Straight	Carbon	Circular	10	0.018	590	0.42	35
	F9	Straight	Carbon	Circular	18	0.017	1770	0.76	180
	F10	Flat-End	PVA	Rectangular	30	0.55x0.75	900	16.09	29
	F11	Twin-coned End	Steel	Circular	35	1.00	1115	243.90	210

* F4 and F5 fibers are identical; different notation are used to indicate different volume fractions.

FIG. 1. Properties of Fibers Investigated (Sketches Not to Scale)

TABLE 1. Mix Proportions

Mix (1)	Cement type 1 (kg/m ³) (2)	Silica fume (3)	10-mm aggregate (4)	Sand (5)	Water (6)	Fibers (7)	Super-plasticizer (8)	Air entrainer (9)	Fiber Volume Fraction (%)	
									Original (10)	In-place ^a (11)
M0 ^b	400	40	265	1,400 ^c	181	—	4.85	0.1	—	—
MF1	400	40	265	1,400	181	60	4.85	0.1	0.77	0.64
MF2	400	40	265	1,400	181	60	4.85	0.1	0.77	0.59
MF3	400	40	265	1,400	181	60	4.85	0.1	0.77	0.64
MF4	400	40	265	1,400	181	9	4.85	0.1	1.00	0.96
MF5	400	40	265	1,400	181	13.5	4.85	0.1	1.50	1.43
MF6	400	40	265	1,400	181	13.5	4.85	0.1	1.50	1.19
MF7	400	40	265	1,400	181	13.5	4.85	0.1	1.50	1.12
MF8	900	135	—	900 ^d	362	33	16.2	0.1	2.00	2.00
MF9	900	135	—	900	362	37	16.2	0.1	2.00	2.00
MF10	400	40	265	1,400	181	10	4.85	0.1	0.77	0.68
MF11	400	40	265	1,400	181	60	4.85	0.1	0.77	0.55

^aAfter considering rebound.

^bM0—mix with no fiber. MF1—mix with fiber F1, etc.

^cConcrete sand.

^d2.5 mm forestry sand.

simply supported, Fig. 2, on all four edges on a rigid support frame with an unsupported middle area of 300 × 300 mm. The load was applied using a circular 100 mm diameter loading cylinder at the rate of 0.28 kN/s and the applied load and load-point-displacement plots were acquired at an acquisition frequency of 1 Hz.

Impact Tests on Beams

Impact tests on the beams were carried out in three-point flexure on a span of 300 mm as shown schematically in Fig. 3. These tests were performed in an instrumented drop-weight impact machine with details of its design, operation, and specimen support system provided elsewhere (Banthia et al. 1989). The machine has a 60.3 kg hammer that was dropped from a height of 0.45 m in a test. At this drop height, the hammer

had a potential energy of 266 J, and an approach velocity of 2.97 m/s just before striking the specimen. This produced an approximate average stress-rate of 28,830 MPa/s (corresponding strain rate ≈ 0.71/s), and with the static stress-rate of 0.012 MPa/s as described above, an impact to static stress-rate ratio of 2.4×10^6 . The knife-edge striking end of the hammer (called the “tip”) carries a load cell, which continuously records the contact load-time pulse between the specimen and the hammer. An accelerometer glued to the bottom of the beam at midspan, recorded the specimen accelerations during an impact. Data from the load cell and the accelerometer were recorded at 10 μs intervals using a PC-based data acquisition system. Some typical time-based plots of load and acceleration are shown in Fig. 4. These were further analyzed by performing a complete dynamic analysis of the event including the

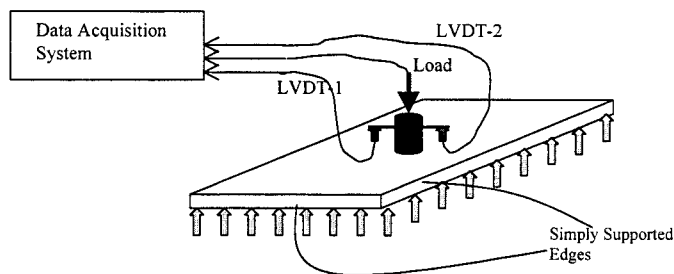


FIG. 2. Schematic of Static Load Application on Plates

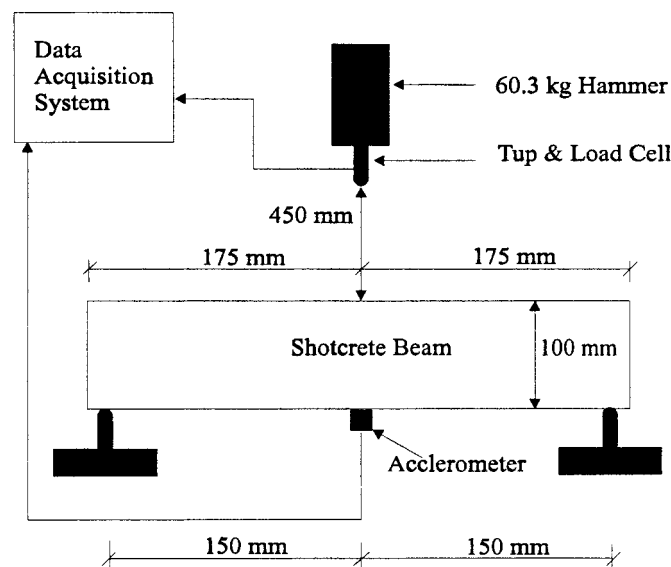
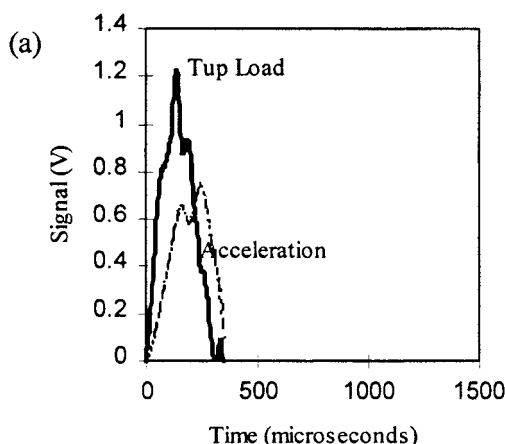


FIG. 3. Schematic of Impact Load Application on Beams

inertial load correction as described in detail elsewhere (Banthia et al. 1989). Briefly, if one can assume that the acceleration distribution along the length of the specimen is linear, then using the principal of virtual work, one can show that the generalized inertial load on the specimen during the impact is

$$P_i(t) = \rho A \cdot \ddot{u}_o(t) \left[\frac{1}{3} + \frac{8(oV)^3}{3l^2} \right] \quad (1)$$

where $\ddot{u}_o(t)$ = midspan acceleration of the beam at time t ; ρ = mass density; and A = cross-sectional area of the beam; l = clear span of the beam; and oV = length of overhanging portion of the beam.



The generalized bending load ($P_b(t)$) then can be obtained from dynamic equilibrium

$$P_b(t) = P_i(t) - P_l(t) \quad (2)$$

where $P_l(t)$ is the recorded hammer (tup) load. The velocity and displacement histories at the load-point can be obtained by integrating the acceleration history with respect to time. If $\dot{u}_o(t)$ is the velocity at the load-point, and $u_o(t)$ is the displacement at the load-point, then

$$\dot{u}_o(t) = \int \ddot{u}_o(t) \cdot dt \quad (3)$$

$$u_o(t) = \int \dot{u}_o(t) \cdot dt \quad (4)$$

Using $P_b(t)$ and $u_o(t)$, the applied (stressing) load versus load-point displacement plots under impact can be obtained, which can then be compared directly with the static load-displacement plots obtained from the companion slow-rate beam tests as per ASTM C1018 described previously.

Impact Tests on Plates

For the impact tests on plates, a support identical to that used in static tests was used. In addition, the rigid steel support frame was securely fixed to the base of the impact machine such that it was fully restrained from moving in either a lateral or vertical direction. While a smaller 1,065 J capacity machine with a 60.3 kg hammer was used for the beams as described previously, a much larger machine with a capacity of about 10,000 J was used for the plate tests (Fig. 5). In this machine, a larger 578 kg hammer can be dropped from variable heights of up to 2.3 m. Detailed description of this impact machine may be found elsewhere (Banthia et al. 1989). For the tests reported here, a hammer drop height of 0.45 m—same as that used for the beam tests—was chosen. At this drop height, the hammer had an approach kinetic energy of 2,551 J, and acquired a velocity of 2.97 m/s just before striking the specimen. In an actual test, the hammer was raised to the appropriate height, and then allowed to fall freely under gravity to strike the simply supported plate at the latter's center. This produced an average loading rate of 104.6×10^4 kN/s, and an impact to static loading-rate ratio of about 3.73×10^6 . The stress-rate ratios (impact/static) used for the plates was, thus, very similar to the one used for the beams (2.4×10^6).

The hammer has a 100 mm diameter cylindrical striker attached to it, which also houses a dynamic load cell that records

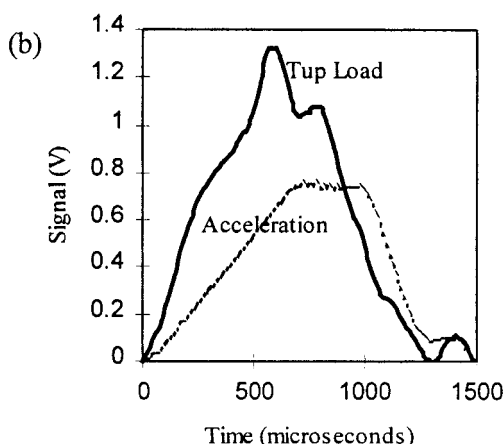


FIG. 4. Tup Load and Midspan Acceleration Signals for: (a) Plain Shotcrete Beam; (b) Steel Fiber Reinforced Shotcrete Beam Reinforced with Fiber F1

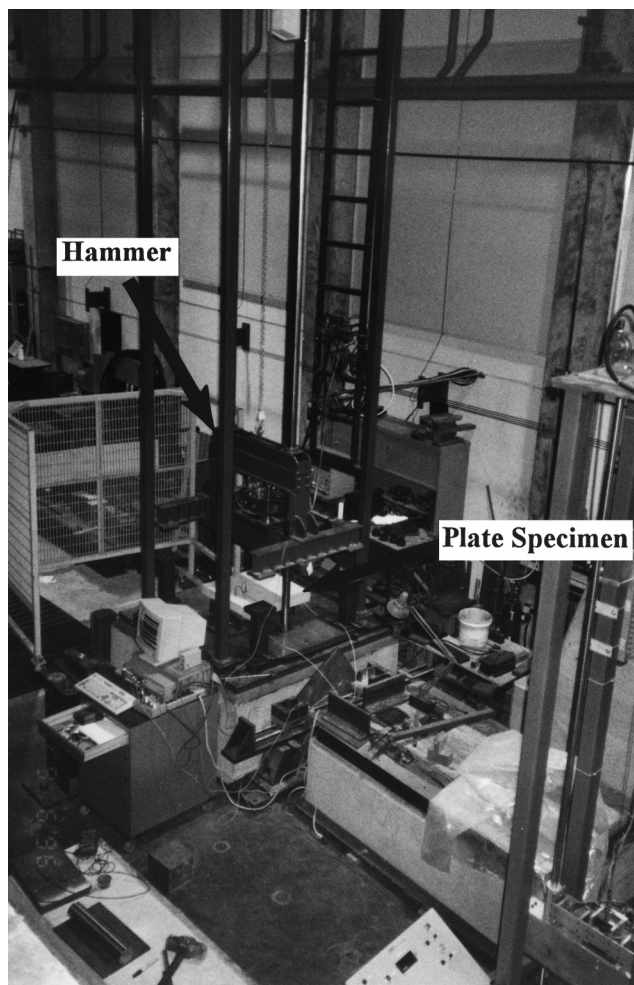


FIG. 5. Instrumented Impact Test Machine with Capacity of ~10,000 J. Machine Has 578 kg Hammer that Was Dropped from Height of 0.45 m on Simply Supported Plate

the contact load versus time pulse generated between the hammer and the specimen during impact. In addition, an accelerometer is glued to the bottom of the plate just under the load point to record the acceleration during impact. Data were recorded at 10 μ s intervals.

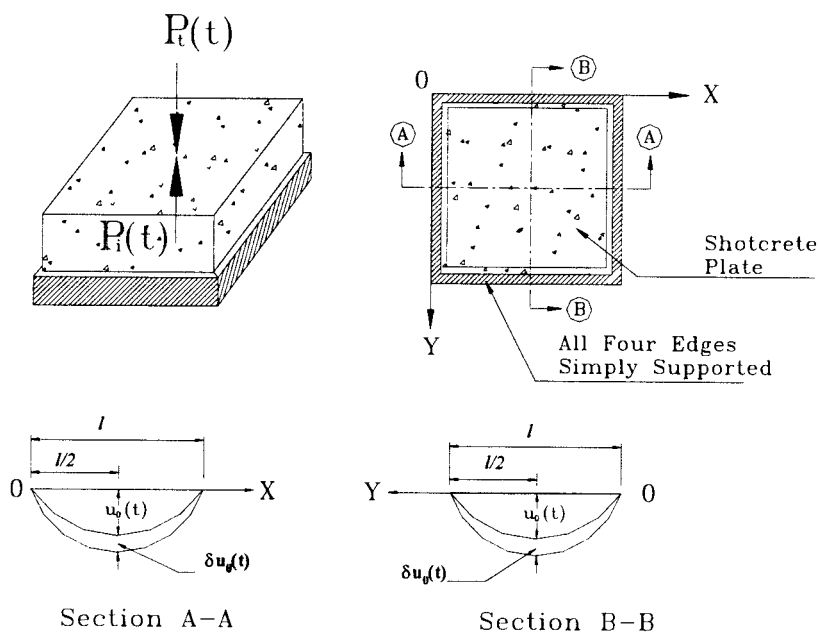


FIG. 6. Analysis Scheme for Plates

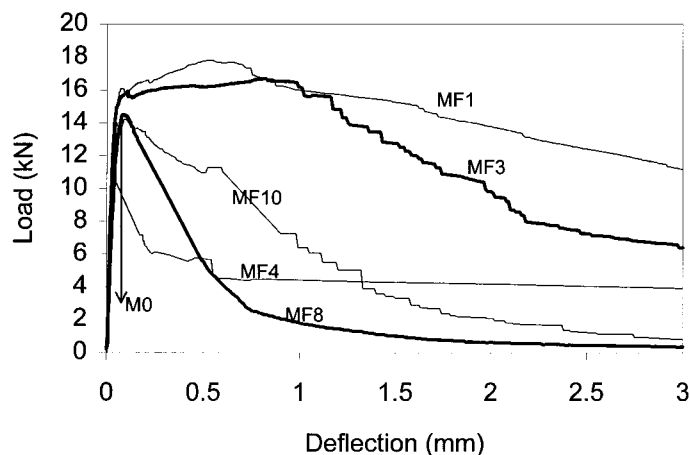


FIG. 7. Static Load-Displacement Plots for Shotcrete Beams Reinforced with Different Fibers (See Table 1 for Fiber Details)

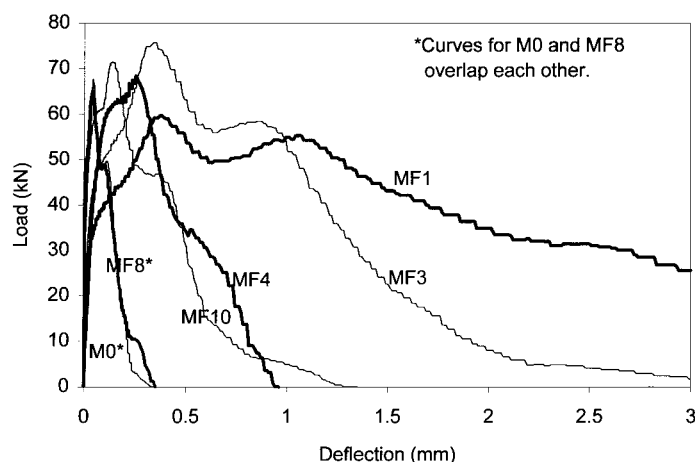


FIG. 8. Impact Load-Displacement Plots for Shotcrete Beams Reinforced with Different Fibers (See Table 1 for Fiber Details)

The contact load-time pulse and the accelerometer data were further analyzed to perform a complete dynamic analysis of the event including inertial load correction with full details given elsewhere (Gupta 1998; Banthia et al. 1999a,b). Briefly, on the basis of an existing analytical solution (Timoshenko

TABLE 2. Static and Impact Data for Shotcrete Beams

Beams (1)	Mix (2)	In-place fiber volume fraction (%) (3)	Compressive strength (MPa) (4)	Flexural Strength			JSCE-SF4 (FT) ^a (To Deflection of 2 mm)		
				Static (MPa) (5)	Impact (MPa) (6)	Ratio impact/static (7)	Static (MPa) (8)	Impact (MPa) (9)	Ratio impact/ static (10)
Plain shotcrete	M0	—	51	4.19	30.49	7.28	0.07	1.49	21.28
Fiber reinforced shotcrete	MF1	0.64	55	5.88	29.75	5.06	5.20	15.65	3.00
	MF2	0.59	54	5.41	40.03	7.40	4.67	18.89	4.04
	MF3	0.64	51	5.55	37.18	6.70	4.75	13.87	2.92
	MF4	0.96	46	4.04	34.08	8.43	1.29	5.71	4.43
	MF5	1.43	45	3.97	34.41	8.67	2.15	11.02	5.12
	MF6	1.19	49	3.96	29.16	7.36	1.47	10.68	7.26
	MF7	1.12	48	3.62	25.89	7.15	1.93	11.55	5.98
	MF8	2.00	52	4.75	33.36	7.02	1.24	1.48	1.19
	MF9	2.00	50	2.79	34.74	12.45	0.07	1.04	14.86
	MF10	0.68	54	4.68	36.78	7.86	2.45	5.47	2.23
	MF11	0.55	53	4.80	22.09	4.60	2.99	7.12	2.38

^aFlexural toughness factor (FT).

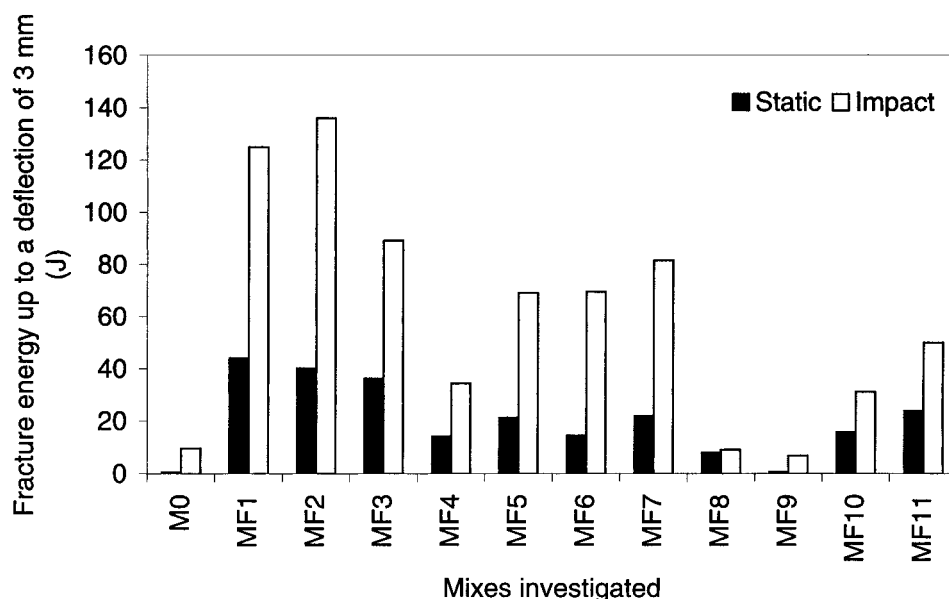


FIG. 9. Fracture Energy Values up to Midspan Deflection of 3 mm for Shotcrete Beams Reinforced with Different Fibers under Static and Impact Loads

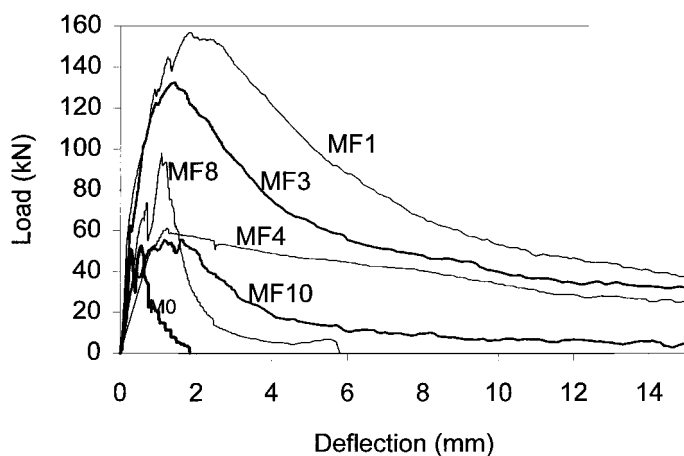


FIG. 10. Static Load-Displacement Plots for Fiber Reinforced Shotcrete Plates with Selected Fiber Types (See Fig. 1 for Fiber Details)

and Woinowsky-Krieger 1970) to the problem of a simply supported plate subjected to a central load and based on observed acceleration distribution profiles, it can be safely assumed that at any instant of time during impact, the acceleration, velocity,

and displacement distributions profiles are sinusoidal along both X and Y axes (Fig. 6). Using the virtual work principle, then, one can show that the generalized inertial load ($P_i(t)$) at the center is given by (Gupta 1998; Banthia et al. 1999a,b)

$$P_i(t) = \rho \cdot h \cdot \ddot{u}_o(t) \cdot \frac{l^2}{4} \quad (5)$$

where ρ = mass density; h = thickness of the plate; and l = width (also length) of the plate. The acceleration at the center of the plate ($\ddot{u}_o(t)$) may be obtained by extrapolating the recorded acceleration at the accelerometer location ($x, l/2$),

$$\ddot{u}_o(t) = \ddot{u}(x, l/2, t) \cdot \operatorname{cosec} \frac{\pi \cdot x}{l} \quad (6)$$

and the generalized inertial point load is given by

$$P_i(t) = \frac{\rho h l^2}{4} \ddot{u}(x, l/2, t) \cdot \operatorname{cosec} \frac{\pi \cdot x}{l} \quad (7)$$

where $\ddot{u}(x, l/2, t)$ is the recorded acceleration at the point ($x, l/2$) on the plate. In this study, however, since the acceleration at the center of the plate was recorded, the generalized inertial load was obtained directly from (5). Once the generalized inertial load is obtained, the plate is modeled as a single degree

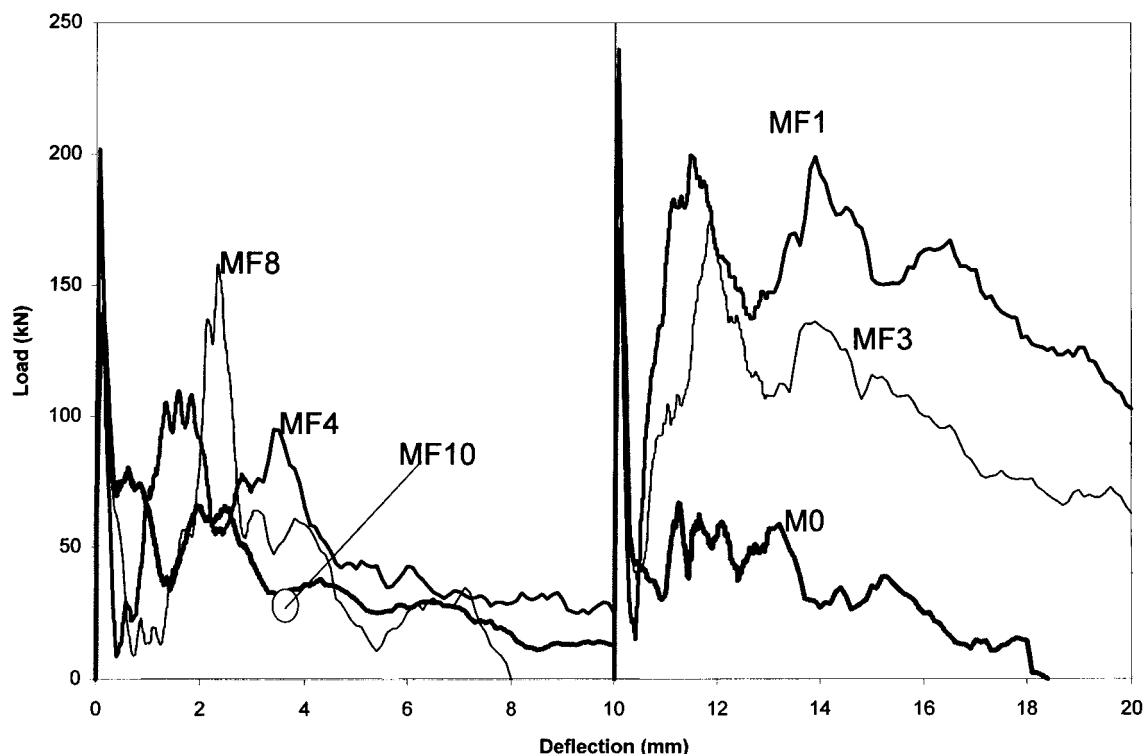


FIG. 11. Impact Load-Displacement Plots for Fiber Reinforced Shotcrete Plates with Selected Fiber Types (See Fig. 1 for Fiber Details)

TABLE 3. Static and Impact Data for Shotcrete Plates: Peak Loads

Beams (1)	Mix (2)	In-place fiber volume fraction (%) (3)	Compressive strength (MPa) (4)	PEAK LOAD				
				Static (kN) (5)	Impact (kN) (6)	Ratio impact/static (7)	Ratio Fiber Reinforced Shotcrete/Plain	
							Static (8)	Impact (9)
Plain shotcrete	—	—	51	52.5	165.5	3.15	—	—
Fiber reinforced shotcrete	F1	0.64	55	157.1	239.9	1.53	2.99	1.45
	F2	0.59	54	130.6	208.8	1.60	2.49	1.26
	F3	0.64	51	132.6	174.4	1.31	2.52	1.05
	F4	0.96	46	61.1	201.9	3.30	1.16	1.22
	F5	1.43	45	89.5	229.4	2.56	1.70	1.39
	F6	1.19	49	65.2	215.2	3.30	1.24	1.30
	F7	1.12	48	68.8	246.6	3.58	1.31	1.49
	F8	2.00	52	98.1	158.0	1.61	1.87	0.95
	F9	2.00	50	48.2	217.7	4.52	0.92	1.31
	F10	0.68	54	55.7	138.9	2.49	1.06	0.84
	F11	0.55	53	104.4	281.0	2.69	1.99	1.69

of freedom (SDOF) system and the generalized bending load can be obtained directly from the equation of dynamic equilibrium as in the case of the beams (2). Further, the velocity and displacement histories at the load-point were obtained by integrating accelerations as before in (3) and (4). Plots of $P_b(t)$, the applied stressing load, and $u_o(t)$, the load-point displacement, were plotted.

RESULTS

Static and Impact Performance of Beams

Some representative static and impact load-deflection curves for beams are shown, respectively, in Figs. 7 and 8. These curves were further analyzed to obtain flexural strengths from the peak load as per ASTM C78 ("Standard" 1994) and the flexural toughness factors (FT) as per JSCE SF-4 ("Method"

1984). These data are given in Table 2. In addition, total fracture energies absorbed to a midspan displacement of 3 mm were calculated.

Based on flexural strengths reported in Table 2, note that under static conditions shotcrete with steel fibers (MF1–MF3, and MF11) demonstrated higher strengths than both the plain shotcrete (MF0) and shotcrete with synthetic fibers (MF4–MF10). Under impact conditions, however, no particular trend among the fibers is noticeable. Also, a substantial increase in the flexural strength occurred under impact loading compared to static loading for both plain and fiber reinforced shotcrete. This has been previously reported for cast cement-based materials (Banthia et al. 1989, 1996). The magnitude of the increase in the strength, however, does not seem to be related either to the presence or absence of fibers or on the type and volume fraction of the fiber. Both plain and fiber reinforced shotcrete beams were also found to be stiffer under impact

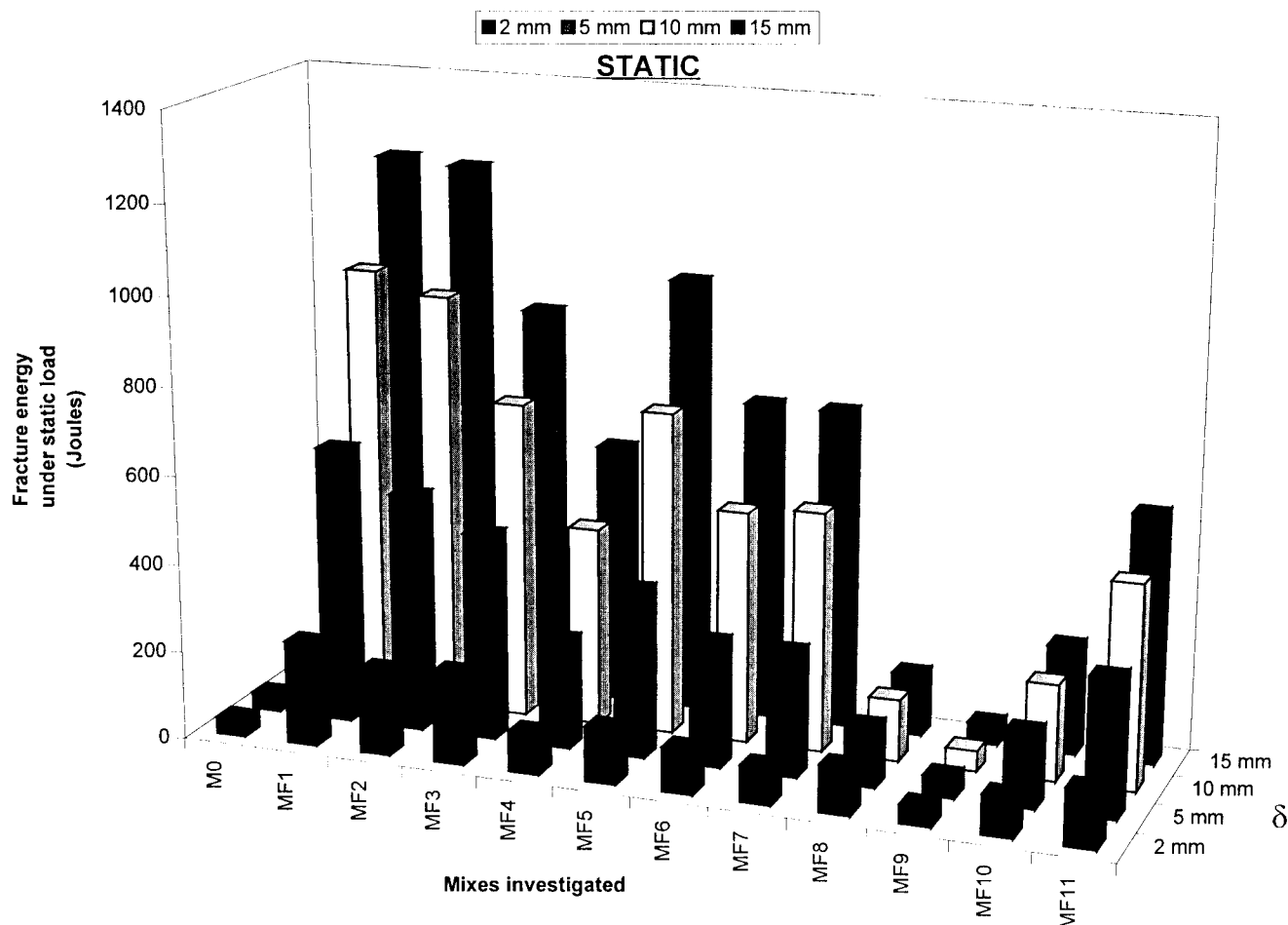


FIG. 12. Fracture Energy Absorption of Plates under Static Loading to Various Deflections

loading compared to static loading. This may be attributed to an increase in the elastic modulus of the matrix under a higher rate of loading as has been reported previously (Watstein 1953). It is worth mentioning here that in this study the specimens were tested in the wet-state soon after their retrieval from the moist room. The high moisture content may be an apparent reason for the particularly pronounced sensitivity to stress-rate (Rossi 1994).

So far as the energy absorption capacity is concerned, notice in Table 2 that the inclusion of fibers improved the flexural toughness factor (FT); the more efficient the fiber, the higher the FT, meaning a higher postcracking residual strength. Notice also an increase in FT under impact loading compared to static loading, implying an enhanced postcracking residual strength of shotcrete under impact. This enhancement is, however, more prominent for plain shotcrete than it is for fiber reinforced shotcrete, an aspect discussed later.

The fracture energy values up to a large (albeit arbitrary) deflection of 3 mm are plotted in Fig. 9. At this displacement, cracks are wide enough, serviceability limit states have been attained, and most fibers have exhausted their stress-transfer capacity across a matrix crack. Inclusion of macrofibers considerably enhanced the energy absorbing capability of shotcrete under static, as well as impact loading. The improvements are, however, more pronounced under static loading.

As seen in Fig. 4(a), for plain shotcrete beams, an impact event lasted for only about 315 μ s. On the other hand, fibers in fiber reinforced shotcrete reduced the stress-intensity at the crack-tip by applying a closing pressure, and as a result the event in the case of fiber reinforced shotcrete beam lasted for

over 1,485 μ s—nearly 4.7 times longer than that for a plain beam.

Static and Impact Performance of Plates

Some representative load deflection plots for plates under static and impact loading are given in Figs. 10 and 11, respectively. These curves were further analyzed to obtain peak loads supported during the tests (Table 3), and fracture energies to small deflections of 2 and 5 mm, and to large deflections of 10 and 15 mm (Figs. 12 and 13).

Under static loading, plates with steel fiber reinforcement (MF1–MF3 and MF11) invariably always supported a much higher load than the plain shotcrete plates (M0) (Table 3). Unlike steel fiber reinforced plates, however, plates with polymeric or carbon fiber (M4–M10) supported loads that are approximately the same or somewhat higher than those supported by the plain, unreinforced plates.

Under impact, both plain and fiber reinforced shotcrete plates exhibited increased peak loads as compared to static loading. Control specimens (M0), and specimens with less efficient fibers, however, generally showed a greater increase in the load carrying capacity under impact. For plates reinforced with steel fibers (MF1–MF3 and MF11), which had already recorded a significant increase in the static load carrying capacity over the unreinforced plates, the corresponding increases under impact loading were not as pronounced. One can deduce, therefore, that the greater the efficiency of a given fiber type in improving the static load carrying capacity, the less pronounced the apparent stress-rate sensitivity under im-

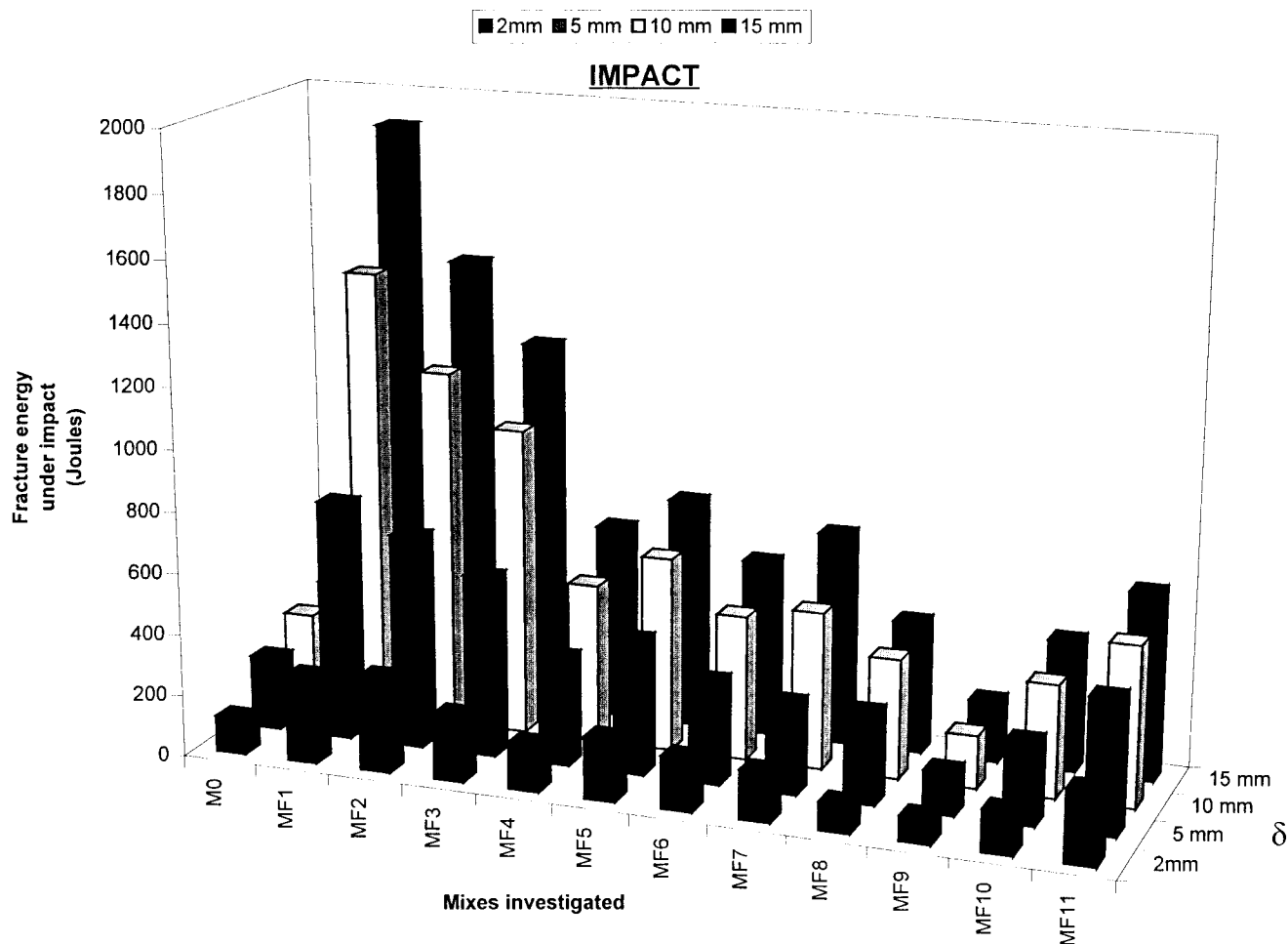


FIG. 13. Fracture Energy Absorption of Plates under Impact Loading to Various Deflections

pact. Finally, it may also be seen in Table 3 that as far as load carrying capacity is concerned, fiber reinforcement is generally more effective under static loading than under impact loading.

As is clear from Figs. 10 and 12, under static loading, all fibers with the exception of the carbon fiber, improved the energy absorption capability of the plain, brittle matrix. The most efficient fiber in this regard is the hooked-end steel fiber, followed by the flat-end steel fiber, the two polypropylene fibers, twin-cone steel fiber, and the PVA fiber, in that order. A similar trend was observed under impact (Figs. 11 and 13). The improvements due to fiber reinforcement, however, were much more pronounced under static loading as compared to impact loading. Energy absorbed by plates under impact was reasonably close to that absorbed under static loading, except in the case of plain (M0) and carbon microfiber (MF8 and MF9) reinforced plates, which absorbed on a proportional basis much greater energy under impact as compared to static loading.

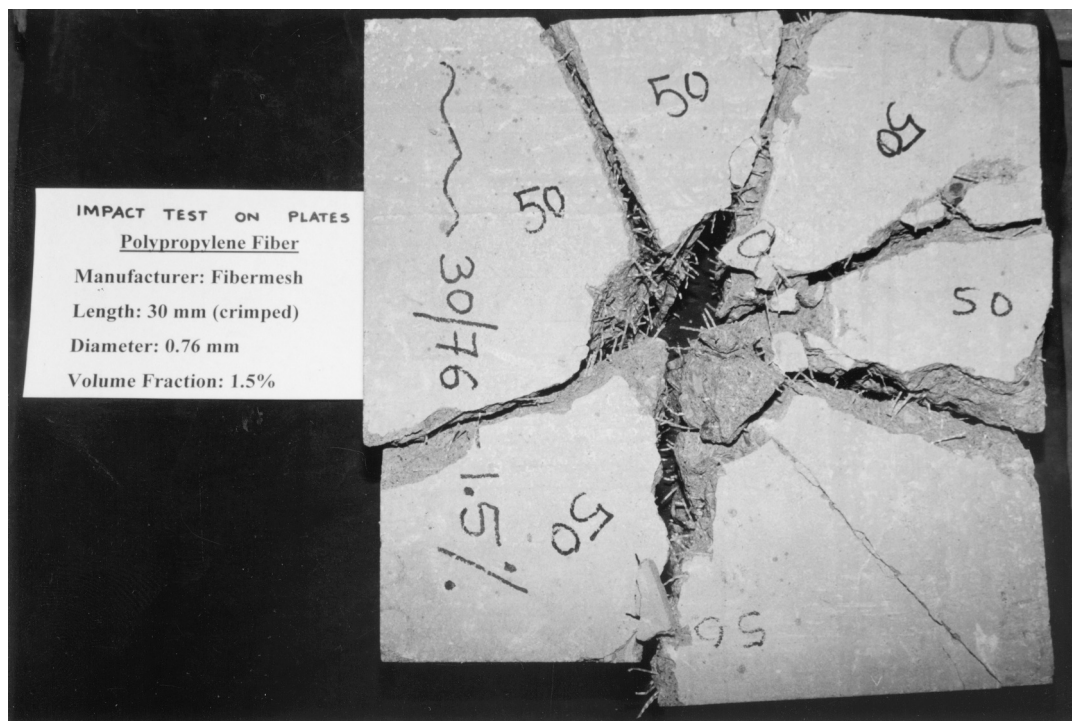
Although the polymeric fibers, as mentioned previously, did not substantially improve the load-bearing capacity of the plates under static loading, they did augment adequately the toughness and energy absorption capability of the plates. However, when compared to most steel fibers, polymeric fibers appear to be far less effective in increasing the energy absorption capacity under impact (Fig. 13). A visual observation of the fractured surfaces revealed that the mode of failure of polypropylene fibers (M4–M7) had changed from complete pull-out to tensile fracture when the rate of loading was changed from static to impact. For the polyvinyl alcohol fiber (M10),

brittle fiber fractures under transverse shear occurred under both rates of loading. Some fractured plates with polypropylene and steel fiber reinforcement are shown in Figs. 14(a and b). Generally, as opposed to plates with the polypropylene fiber, plates with the steel fiber (F1) maintained their structural integrity after impact loading. This is also observable based on the residual load carrying capacity of such plates in Fig. 11.

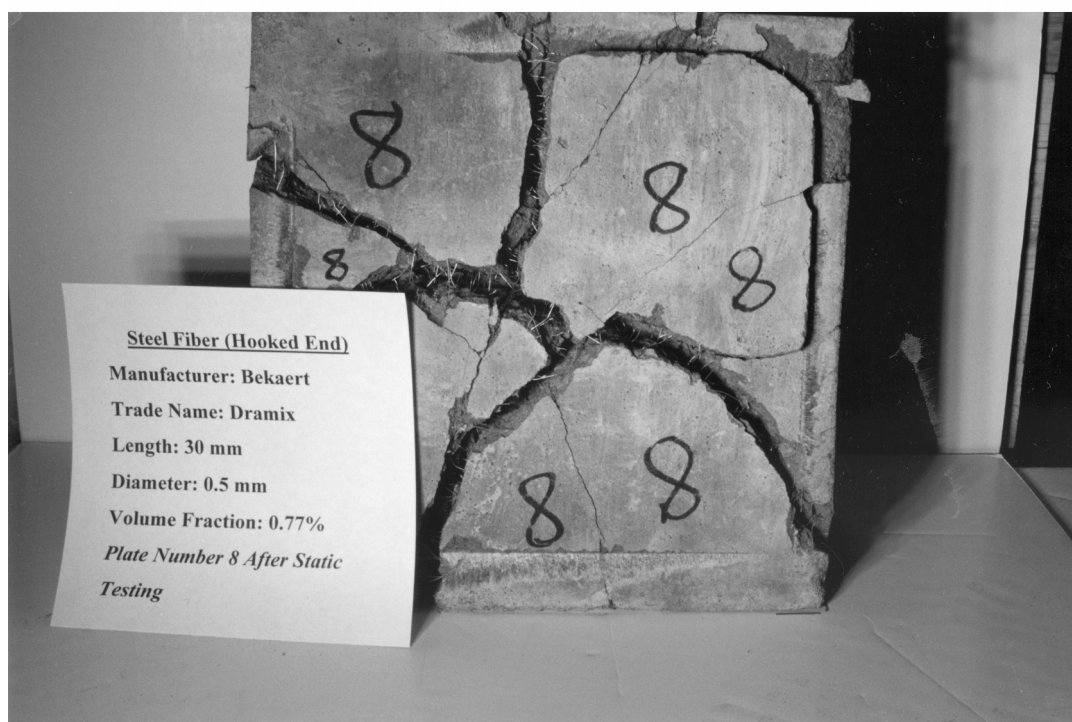
Comparison between Plates with Beams

In Fig. 15 some typical beam and plate curves for fibers F1, F3, and F8 are compared under static loading. In Fig. 16, the control matrix (M0) and fibers F4 and F10 are compared, once again, under static loading. Notice that in the beam tests all the specimens supported, more or less, the same peak load, whereas in the plate tests the specimens reinforced with fibers sustained a higher load than the control, and the plates with the highly efficient steel fibers (F1 and F3) sustained much higher loads than the control (M0). Comparing the plots for plates with fibers, it is clear that the peak load sustained in these tests is in itself a strong indicator of the fiber's reinforcing efficiency, something not possible in the beam tests. In other words, the ability of an efficient fiber to reinforce is further magnified and clearly visible in a plate test.

Beams and plates do not always produce consistent trends. For example, as seen in Fig. 15, fibers F1 and F3 appear to demonstrate minimal differences in performance based on the beam tests. However, when the plate test results for the same



(a)



(b)

FIG. 14. Bottom Surface of Shotcrete Plate Reinforced with: (a) Polypropylene Fiber (F7) after Impact Loading; (b) Hooked-End Steel Fiber (F1) after Static Loading

two fibers are compared, their performances differ significantly. Further, in Fig. 16, the trends observed on the basis of beams for fibers F4 and F10 appear to be reversed in the case of plates. This is of concern given that both these tests are being proposed for standardization, and may predict different trends when different fibers are compared. In reality, however, since shotcrete is usually applied as a thin two-dimensional lining, and on the basis of Table 3, one can easily see that with the exception of the plain matrix, plates are not as sensitive to the applied stress-rate as the beams. Therefore, the

plate specimens appear to be a more logical choice for characterizing the toughness of fiber reinforced shotcrete.

CONCLUSIONS

1. In the case of wet-mix shotcrete, fiber reinforcement is highly effective in improving the fracture energy absorption and toughness under impact loading. The improvements are, however, not as pronounced as those under static conditions, and highly dependent on the type and shape of the fiber.

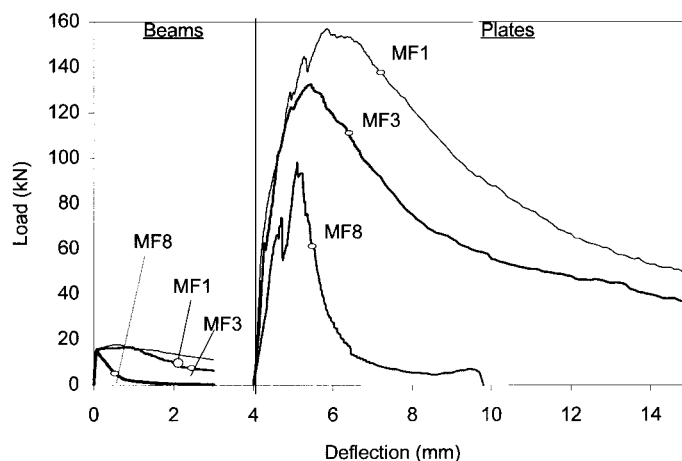


FIG. 15. Comparison between Static Load-Displacement Plots for Plates and Beams (Fibers F1, F3, and F8)

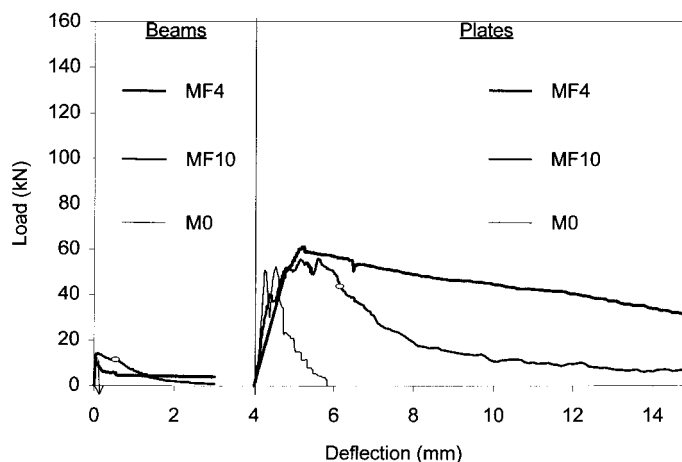


FIG. 16. Comparison between Static Load-Displacement Plots for Plates and Beams (Fibers F4 and F10)

- Like other cement-based materials, wet-mix shotcrete (both plain and fiber reinforced) is highly sensitive to the rate at which the load is applied. Both plain and fiber reinforced shotcrete are stronger, stiffer, and tougher under impact loading than under static loading.
- When beams and plates are compared, it is evident that the two specimen geometries do not always produce consistent trends, and this appears to be true under both static and impact conditions. Given the loading conditions in reality and the relatively stress-rate insensitive nature of plates, however, a plate specimen appears to be the preferred choice.

APPENDIX. REFERENCES

- Banthia, N., Mindess, S., Bentur, A., and Pigeon, M. (1989). "Impact testing of concrete using a drop-weight impact machine." *Experimental Mech.*, 29(2), 63–69.
- Banthia, N., Trottier, J.-F., and Beaupré, D. (1994). "Steel fiber reinforced shotcrete: Comparisons with cast concrete." *J. Mat. in Civ. Engrg.*, ASCE, 6(3), 430–437.
- Banthia, N., and Trottier, J. F. (1995). "Test methods for flexural toughness characterization of fiber reinforced concrete: Some concerns and a proposition." *ACI Mat. J.*, 92(1), 48–57.
- Banthia, N., Mindess, S., and Trottier, J. F. (1996). "Impact resistance of steel fiber reinforced concrete." *ACI Mat. J.*, 93(5), 472–479.
- Banthia, N., Gupta, P., and Yan, C. (1999a). "Impact resistance of fiber reinforced wet-mix shotcrete, Part 1: Beam tests." *RILEM, Mat. and Struct.*, Vol. 32, Oct., 563–570.
- Banthia, N., Gupta, P., and Yan, C. (1999b). "Impact resistance of fiber reinforced wet-mix shotcrete, Part 2: Plate tests." *RILEM, Mat. and Struct.*, Vol. 32, Nov., 643–650.
- Bernard, E. S. (1997). "The influence of edge-restraint on flexural behavior in square SFRC slabs." *Engrg. Rep. No. CE5*, University of Western Sydney.
- "European specification for sprayed concrete." (1996). EFNARC.
- Gupta, P. (1998). "Impact resistance of fiber reinforced wet-mix shotcrete," M.A.Sc. thesis, Univ. of British Columbia, Vancouver, Canada.
- Kirsten, H. A. D. (1997). "Fiber-reinforced shotcrete." *World Tunneling*, (Nov.), 411–414.
- "Method of test for flexural strength and flexural toughness of fiber reinforced concrete." (1984). *SF4*, Japan Society of Civil Engineers, 45–51.
- Rossi, P. (1994). "Dynamic behavior of concretes: From the material to the structure." *Mat. and Struct.*, RILEM, Paris, 27, 319–323.
- "Standard test method for flexural toughness and first crack strength of fiber reinforced concrete." (1996). *C 1018-96*, ASTM, West Conshohocken, Pa., 506–513.
- "Standard test method for flexural strength of concrete (using simple beam with third-point loading)." (1994). *C-78-94*, ASTM, West Conshohocken, Pa.
- Timoskenko, S., and Woinowsky-Krieger, S. (1970). *Theory of plates and shells*. McGraw Hill, New York.
- Watstein, D. (1953). "Effect of straining rate on the compressive strength and elastic properties of concrete." *J. Am. Concrete Inst.*, 49(8), 729–756.